Nuclear Materials and Energy 000 (2016) 1–6

Contents lists available at ScienceDirect

Nuclear Materials and Energy

journal homepage: www.elsevier.com/locate/nme

Cracking behavior of tungsten armor under ELM-like thermal shockloads II: A revised prediction for crack appearance map

Muyuan Li, Jeong-Ha You*

Max-Planck-Institut für Plasmaphysik, Boltzmannstr. 2, 85748 Garching, Germany

ARTICLE INFO

Article history:
Received 20 November 2015
Revised 3 February 2016
Accepted 4 February 2016
Available online xxx

Keywords:
Divertor
Tungsten armor
ELM-like thermal shock
Cracking, High-heat-flux loads
Residual stress

ABSTRACT

In this work, the surface cracking features of tungsten armor under thermal shock loads by edge-localized mode (ELM) were investigated by means of computational fracture mechanics analysis. For the simulation it was assumed that a small crack was initiated at low temperature after the shut-off of thermal load in contrast to the previous studies where the presence of a crack before thermal loading was assumed. The threshold power density for surface cracking was predicted to range between 0.3 and 0.6 GW/m^2 while the threshold of base temperature lay between 200 and 400 °C. The theoretically predicted damage map agreed well with the experimental data from electron beam irradiation tests. The current simulation model turned out to match better to the real experimental observation than the previous predictions where the threshold base temperature lies roughly between 400 and 600 °C.

1. Introduction

Tungsten has been considered as the most promising armor material for plasma-facing components (PFCs) in fusion reactors such as divertor target and first wall. In the fusion reactor, the tungsten-armored PFCs shall be subjected to significant surface heat flux loads due to radiation and particle bombardment from the plasma. In ITER and DEMO, the stationary heat flux load is expected to reach 10 MW/m^2 during normal plasma operation and up to 20 MW/m^2 during slow transients [1]. On the other hand, a large amount of energy is deposited onto local areas of the armor surface in a very short period. Such transient thermal loads are induced by different types of plasma instability taking place during tokamak operation (e.g. ELMs) [2]).

There are plenty of experimental reports on the detrimental impact of intense transient thermal shock loads on the tungsten-based materials where the thermal shock loads were simulated by means of high power electron beam or hydrogen beam with short pulses. One of the pioneering works on this topic is the ELM-like thermal shock tests using electron beam irradiation by Linke and coworkers [3–5]. Under typical ELM-like thermal shock conditions (~1.3 GW/m^2), they observed a systematic trend of damage formation and evolution on the heat-loaded surface. Typical damage features were surface cracking or surface roughening due to plastic deformation. The patterns and severity of damage showed a clear dependence on the deposited power density, base temperature of armor samples, number of pulses and material grade. It turned out that there was a threshold in power density and base temperature below which no visible damage was observed. In the literature, analytical studies on cracking condition and numerical prediction of cracking pattern on tungsten surface under high heat flux loads are found [6,7], where the cracking pattern was simulated using a dedicated code (PEGASUS-3D) with the maximum stress-based failure criterion. On the other hand, fracture mechanics-based computational analyses of this topic were recently reported by the present authors where crack tip loads were assessed by means of energy criterion of failure and finite element method. In a series of articles [8–10], they clarified the mechanism of cracking, predicted the cracking paths and patterns and assessed the driving force of crack propagation on the computational basis using finite element analysis (FEA). Finally, they could construct a damage map as a function of power density and base temperature which agreed fairly well with the experimental data.

In the previous studies, a pre-existing surface crack was assumed in the model prior to thermal loading. This resulted in a significant overestimation of the crack tip loads (J-integral) for onset of crack leading to a conservative estimation of the damage thresholds. In this work, a more realistic simulation was carried out by assuming crack initiation after cooled down to the base temperature (that is the end of passive cooling). Comparative

* Corresponding author. Tel.: +49 89 3299 1373.
E-mail address: you@ipp.mpg.de (J.-H. You).

http://dx.doi.org/10.1016/j.nme.2016.02.001

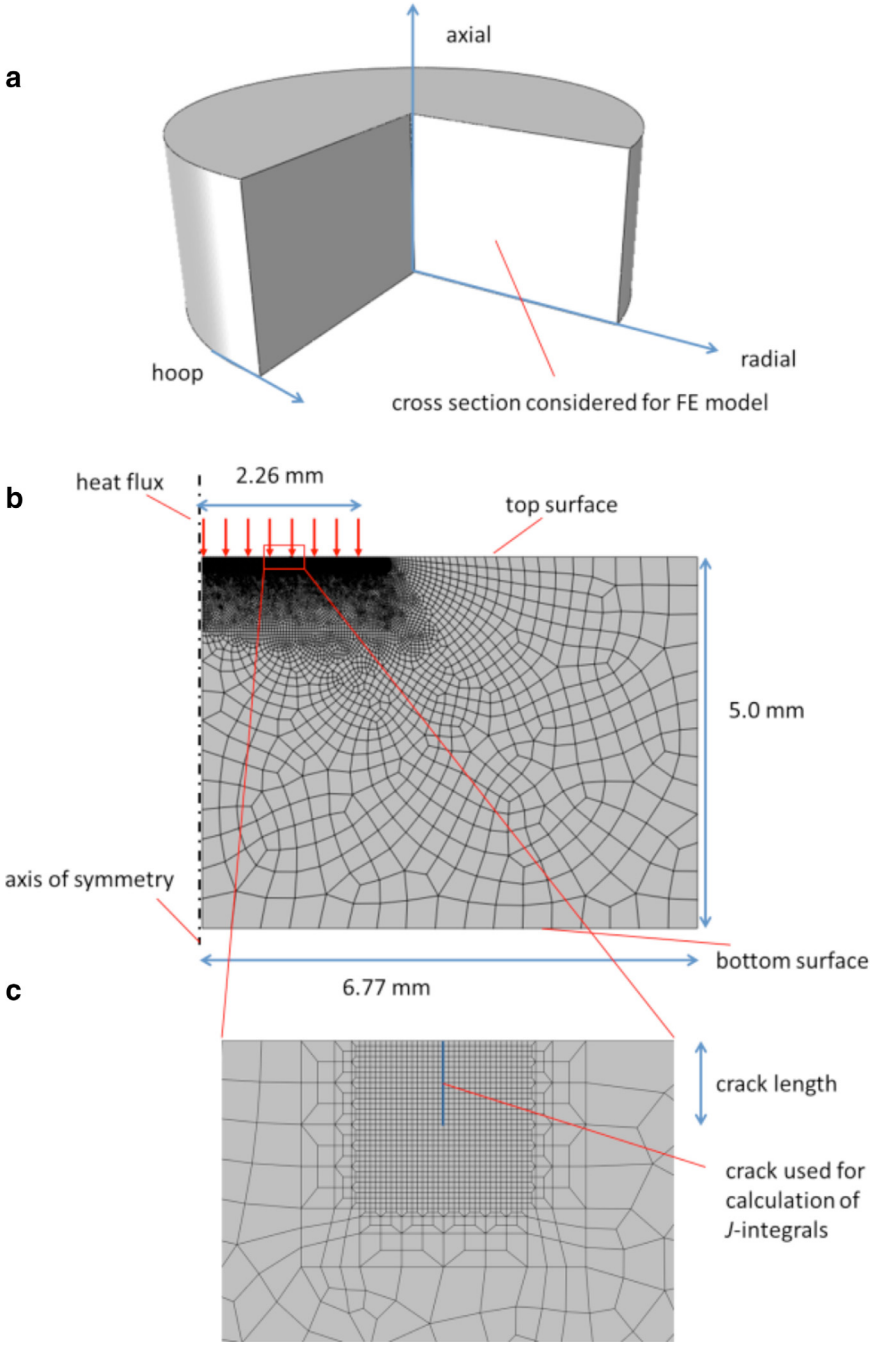

Fig. 1. (a) Schematic illustration of the model geometry, (b) two-dimensional FE model created for the right half of the vertical cross section. The mesh consists of axisymmetric elements reflecting the rotational symmetry of the model, (c) refined mesh in the vicinity of the crack. .

estimations of the *J*-integrals and the damage thresholds are presented for the two different crack initiation models. A new damage map is produced for a wide range of ELM-like thermal shock loading parameters.

2. Finite element modeling

The finite element (FE) model used for this study was created considering the typical test settings applied for the thermal shock experiments carried out at electron beam irradiation facility JUDITH in Forschungszentrum Jülich. The reference geometry considered for the FE model is a disk-shaped sample of tungsten armor. For simplicity, a reduced dimension of Ø 6.7 mm × 5 mm was used instead of the original sample size of 12 mm × 12 mm × 5 mm (see Fig. 1(a)). In the analysis, a simplified two-dimensional axisymmetric FE model was used which represents the right half of the vertical cross section with the left edge as the rotational symmetry axis (see Fig. 1(b)). The simulation tool was the commercial FEM code ABAQUS [11]. The FE model consists of 15,000 linear quadrilateral elements. The mesh was sufficiently refined in the vicinity of the pre-crack where the element size was reduced down to 1.25 μm (see Fig. 1(c)). A pre-crack positioned 1.2 mm away from the center of the heat-loaded area is chosen as a typical crack appearing within the heat-loaded area [10]. The material properties [12,13] used in this study are listed in Table 1.

Please cite this article as: M. Li, J.-H. You, Cracking behavior of tungsten armor under ELM-like thermal shockloads II: A revised prediction for crack appearance map, Nuclear Materials and Energy (2016), http://dx.doi.org/10.1016/j.nme.2016.02.001

Table 1
Properties of tungsten at selected temperatures [12,13].

	20 °C	400 °C	1200 °C	2000 °C
Young's modulus (GPa)	398	393	256	285
Yield stress (MPa)	1384	947	346	57
Heat conductivity (W/m K)	173	140	105	99
Specific heat (J/kg K)	129	141	163	180
Coefficient of thermal expansion (10^{-6}/K)	4.5	4.63	4.98	5.43
Density (kg/m^3)	19.3	19.2	19.0	18.7

In this work, two cases of crack initiation scenarios are assumed, namely, 1) a crack is pre-existing already prior to thermal loading, 2) a crack is initiated after the sample is cooled down (i.e. at the end of cooling stage). For modeling, a small crack (initially 20 μm long) is created into the armor surface either before thermal loading or after cooling, respectively. To calculate the *J*-integral for the pre-crack inserted at the end of cooling, the stress fields calculated for a crack-free body is read into the model as initial conditions for the subsequent fracture mechanics analysis. In both cases, it was verified that the *J*-integral values exhibit the required path independence. The simulation procedure is as follows: (1) transient thermal conduction analysis to calculate the temperature evolution, (2) elasto-plastic analysis to calculate the thermal stress and plastic strain (with or without a pre-crack), (3) elasto-plastic analysis to calculate the elastic recovery and residual stress on the basis of the crack-free stress field imported from step 2 (with a pre-crack), and (4) post-processing to calculate the crack tip loading (*J*-integral) in steps 2 and 3. *J*-integral is a measure of the driving force for crack extension. If the magnitude of *J*-integral for a pre-crack is larger than the critical value (i.e. fracture energy), the pre-crack is supposed to extend to a finite length. *J*-integral attains its maximum value under tensile crack tip load during cooling. The virtual crack extension technique was employed to compute the *J*-integral within the framework of FE formulation.

It should be noted that the axi-symmetric two-dimensional model used here can produce only circular cracks, and such a crack configuration does not fully match the actual crack network pattern observed. However, the largest driving force for cracking is dominated by the radial component of tensile residual stress. This means, surface cracks are bound to initiate firstly along the hoop direction with regard to the beam axis. Furthermore, the crack length considered in this work is very short, so the *J*-integral estimated from the two-dimensional model could be regarded as a good indicative estimate for the real cases and a reasonable compromise between computational costs and accuracy.

3. Results and discussion

Fig. 2 shows the temperature and the residual stress field produced in the near-surface region of tungsten armor at the power density of 1.27 GW/m^2 at a base temperature of 20 °C. It is seen that an extremely steep temperature gradient builds up within the depth of 1 mm where the temperature difference in the vertical direction is larger than 2000 °C and the surface temperature reaches 2660 °C. The very strong temperature gradient has a nonlinear profile as it is generated by a transient thermal load thus inducing thermal stress. The very high temperature near the surface produces large thermal expansion strain locally near the surface within the heat flux loading area. On the other hand, the surrounding region remains only in a relatively cold state as the pulse duration time is not long enough to allow long range heat conduction for uniform heating. The cold surrounding material is hardly strained as the temperature change is negligibly small. Thus, the surrounding region acts as a kinematic constraint. This large mismatch in thermal strain causes strong thermal stress which readily leads to plastic yielding of the material within the high-heat-flux-loaded region because the yield stress (and flow stress) of tungsten at such a high temperature is considerably reduced to a low stress level. Upon cooling the surface temperature decays very fast by outward heat conduction. The entire tungsten armor begins to undergo prompt elastic recovery, but the surface layer which has already deformed plastically during heating phase cannot fully recover the original shape due to the permanent deformation whereas the surrounding region is able to achieve complete elastic recovery theoretically and thus tries to reach the original state. After the overall cooling, there is a big mismatch in the residual strains between the heat loaded surface region and the surrounding region. This strain mismatch produces a thermo-plastically induced residual stress field as shown in Fig. 2. During the high-heat-flux heating the surface layer experiences strong compressive thermal stress as the excessive local thermal expansion of the hot surface is partially restrained by the relatively colder bulk material surrounding the heat-loaded area. Owing to the very high surface temperature and thus significantly reduced yield stress, the surface layer undergoes plastic yield under compression while the rest part remains still elastic. Upon turning-off of the heat flux pulse, the material is cooled down rapidly where the surrounding bulk material tries to recover its original geometry elastically. The heat-loaded surface region, however, cannot follow this elastic recovery due to plastic deformation and is pulled out by the elastic restoring force of the surrounding bulk producing tensile residual stress locally. It turns out that the tensile residual stress in the surface layer is higher than 1200 MPa which is strong enough to cause cracking. If there were a small pre-existing crack or fault on the surface, the

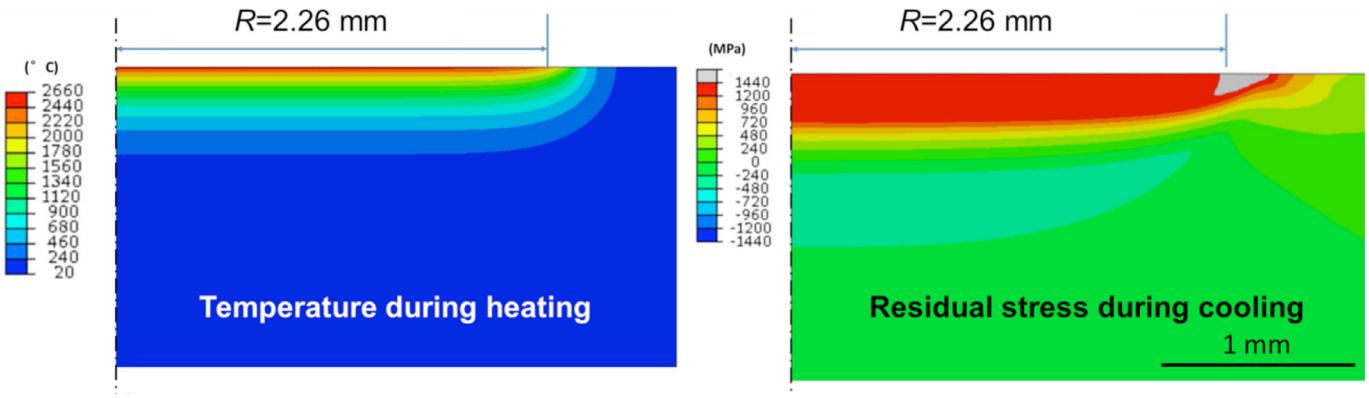

Fig. 2. Temperature and residual stress field computed for the deposited thermal power density of 1.27 GW/m^2 at a base temperature of 20 °C [10].

Please cite this article as: M. Li, J.-H. You, Cracking behavior of tungsten armor under ELM-like thermal shockloads II: A revised prediction for crack appearance map, Nuclear Materials and Energy (2016), http://dx.doi.org/10.1016/j.nme.2016.02.001

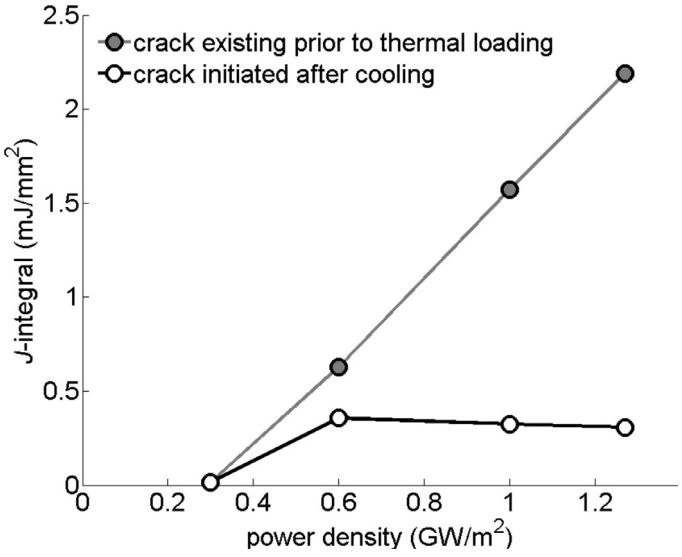

Fig. 3. *J*-integral values of a pre-existing surface crack formed prior to thermal loading and of a crack initiated after cooling plotted as a function of deposited power density (crack length: 20 μm, base temperature: 20 °C).

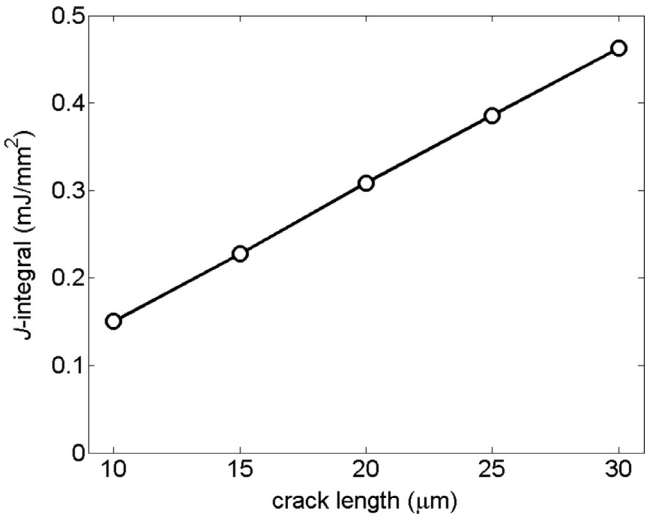

Fig. 4. *J*-integral values of a surface crack initiated after cooling with different size (heat flux density: 1.27 GW/m^2).

driving force of cracking can be very high leading to further crack growth. Since such a surface cracking phenomenon aggravates s the erosion and damage of tungsten armor significantly under repeated thermal shock loads, careful attention needs to be paid in terms of its mechanism and impact. To this end, fracture mechanics can provide rigorous quantitative assessment of cracking behavior.

Fig. 3 shows the estimated *J*-integral values of a surface crack (length: 20 μm, base temperature: 20 °C) as a function of deposited power density. The two data sets indicate the two cases of crack initiation, namely, before the thermal shock loading and at the end of cooling, respectively. The two crack initiation cases show a completely different trend from each other. The *J*-integral for the pre-crack inserted before thermal loading increases proportionally with the increasing power density. At 1.2 GW/m^2 the *J*-integral reaches ca. 2 mJ/mm^2. On the contrary, the *J*-integral for the crack created after cooling increases initially only up to 0.6 GW/m^2, then readily reaches saturation even exhibiting a slight decrease under higher heat flux loads. The *J*-integral for the crack forming at the end of cooling is significantly lower than that of the pre-existing crack. This feature indicates that the assumption of a pre-existing surface crack being present prior to thermal shock loading leads to a significant overestimation of the crack tip loads for crack growth compared to the case of the initially flaw-free surface which is to undergo crack initiation after cooling. Once a crack has been formed on the surface under repeated thermal shock loads, then the *J*-integral estimates obtained for the pre-existing crack would be valid for the real situation.

The deviating *J*-integral behavior can be interpreted in terms of stress and strain evolutions near the crack tip. When there is a pre-crack prior to thermal loading, the plastic strains and the plastic dissipation energy produced during the loading and cooling period contributes to the magnitude of *J*-integral [14]. The accumulated plastic strain increases with increasing the power density, so *J*-integral increases with increasing the power density as well. If a crack is initiated after cooling, the crack tip load is affected mainly by the plastic residual stress field. As at the power density of 0.6 GW/m^2 or above, the residual stress is nearly constant in the central part of loading area, the *J*-integral is roughly constant as well. At the power density of 0.3 GW/m^2, plastic strain nearly vanishes during whole loading and cooling phase, thus the *J*-integral converges nearly to null for both cases.

The residual stress field plotted in Fig. 2 manifests clearly that the strong tensile stress field produced during cooling phase is the major driving force for crack growth of a surface crack. On the other hand, the fracture toughness of tungsten decreases significantly after cooling when the surface temperature rapidly drops down below the ductile-to-brittle transition temperature (DBTT). The fracture toughness reduction promotes brittle cracking in the cold state after cooling. Initiation or propagation of a surface crack is not plausible before that since compressive stress prevails in the surface layer while the very high temperature keeps the material in the surface layer ductile and soft.

In Fig. 4 the *J*-integral values of a surface crack initiated after cooling are plotted for five different crack sizes ranging from 10 to 30 μm. The *J*-integral data indicate the maximum values occurring at the end of cooling after the heat flux loading at 1.27 GW/m^2. The *J*-integral is shown to linearly increase as the surface crack grows at least up to the depth of interest. This linearly proportional dependence is due to the fact that the tensile residual stress in the near-surface region (up to the depth of 200 μm) is nearly uniform in the depth direction [10]. If the applied stress is uniform, the strain energy release rate at the crack tip (proportional to the square of the stress intensity factor) is directly proportional to the crack size. Fig. 4 indicates that once the crack has been infinitesimally extended, the growth process will progress by itself further even though the heat flux loads remains same, if the momentary *J*-integral is larger than the critical value. It is noted that the length range of crack size considered in Fig. 4 represents the mean size of typical grains in the tungsten samples used for the thermal shock test experiment.

Fig. 5 shows the *J*-integral values of a surface crack initiated at the end of cooling plotted as a function of power density ranging from 0.3 to 1.27 GW/m^2 and for five different base temperatures ranging from 20 °C to 800 °C. Here, the crack size assumed is 20 μm. Except for the lowest power density of 0.3 GW/m^2, the *J*-integral drastically decreases as the base temperature is increased. This thermal relaxation of crack tip load is owing to the reduction of the residual stress with increasing base temperature. At the power density of 0.3 GW/m^2, the residual stress first increases and then subsequently decreases as the base temperature monotonically increases showing a maximum at 600 °C. It is remarkable that, at base temperatures of 600 °C or above, the *J*-integral does

Please cite this article as: M. Li, J.-H. You, Cracking behavior of tungsten armor under ELM-like thermal shockloads II: A revised prediction for crack appearance map, Nuclear Materials and Energy (2016), http://dx.doi.org/10.1016/j.nme.2016.02.001

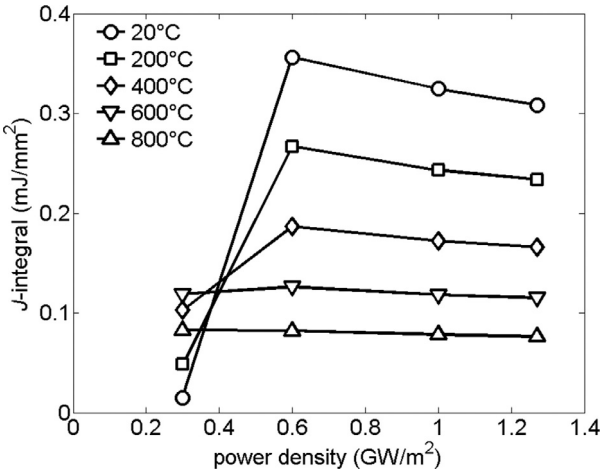

Fig. 5. *J*-integral for a pre-crack of 20 μm as a function of power density (0.3–1.27 GW/m^2) and base temperature (20–800 °C).

Table 2
Critical values of the *J*-integral converted from the fracture toughness data in [15] assuming linear elastic fracture mechanics.

Temperature (°C)	20	200	400	600	800
Critical value of *J*-integral (mJ/mm^2)	0.1549	0.2329	0.4325	0.9582	2.4579

not show any distinctive dependence on the power density for the whole power density range under consideration.

Table 2 lists the critical values of *J*-integral converted from the literature data of fracture toughness [15] assuming linear elastic fracture mechanics (LEFM). This LEFM assumption is a reasonable approximation for the lower base temperatures up to 400 °C above which plastic deformation is the dominant surface damage feature [15]. At higher base temperatures the LEFM conversion may cause an underestimation of fracture resistance.

Fig. 6 presents the crack appearance map plotted for the relevant range of power density and base temperature indicating the thresholds for the critical loading regime where cracks may occur. The threshold parameters were determined by comparing the *J*-integral values of a pre-crack (20 μm) with the critical fracture

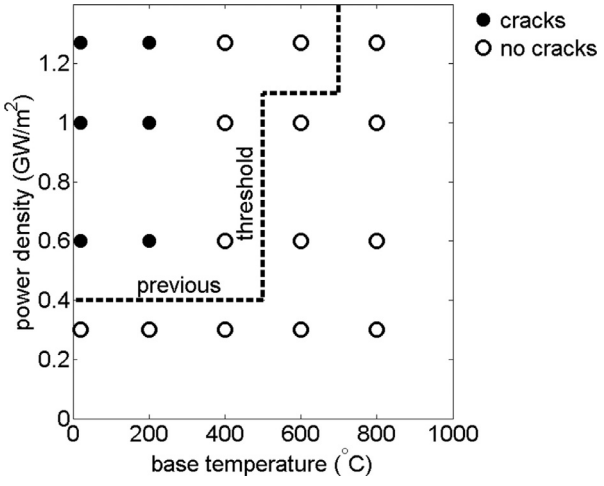

Fig. 6. Crack appearance map plotted for the relevant range of power density and base temperature compared with the previously predicted thresholds for the critical loading regime where cracks may occur.

energy value. It is found that the threshold power density lies between 0.3 and 0.6 GW/m^2, and the threshold base temperature between 200 and 400 °C. This result roughly coincides with the experimental data [3], where the threshold power density for crack formation was between 0.15 and 0.33 GW/m^2 and the base temperature threshold is between 150 and 300 °C. It is also noted that the current damage map matches better with the experimental data than those of the previous study, in which the *J*-integral was assessed for a pre-existing crack only leading to conservative estimation.

The linear dependence of *J*-integral on the crack size as shown in Fig. 4 allows an extrapolation of the map for the cracks with sizes between 20 and 40 μm, which yields approximately the same threshold values as in Fig. 6. For a crack of 10 μm, the base temperature threshold lies between 20 °C and 200 °C, while it is about 400 °C for a crack of 50 μm. It should be noted that the current estimation has been made on the basis of continuum assumption which is surely a rough approximation. Realistic microstructural features would be needed for more accurate assessment.

In this work the model is setup based on the thermal shock test in Forschungzentrum Jülich which does not accurately stand for the real loading situation in a fusion reactor. In the case of real tokamak operation, the heat flux loads generated by ELMs will have a much more diffuse distribution along the poloidal positions, although possibly there will be a peak(s). For cracking simulation for such a case input data of a realistic ELM heat flux footprint would be needed.

4. Conclusions

In this work, the *J*-integral for a tungsten surface crack was computed for a wide range of ELM-like thermal shock loads by means of finite element simulations and fracture mechanics analysis. A comprehensive parametric study was carried out for the power density range of 0.3–1.27 GW/m^2 and the base temperature range of 20–800 °C. Comparative estimations were delivered for two different scenarios of crack initiation, namely, a pre-existing crack present already prior to thermal loading and a crack being initiated after cooling, respectively. Following features of cracking behavior were found:

1. The crack inserted before thermal loading experiences more strain energy than the crack initiated after cooling. The latter one is more suitable for simulating the initial crack occurrence.
2. In the surface layer, the *J*-integral is linearly proportional to the crack size.
3. The threshold power density for surface cracking is predicted to lie between 0.3 and 0.6 GW/m^2, and the threshold base temperature between 200 and 400 °C for surface cracks initiated after cooling (size: 20–40 μm).
4. The predicted threshold values of power density and base temperature for surface cracking agree roughly with the experimental data observed in the electron beam irradiation tests. This revised prediction agrees better with the experimental data than the previous conservative estimations [10].

Acknowledgment

This work has been carried out within the framework of the EUROfusion Consortium and has received funding from the Euratom Research and Training program 2014–2018 under Grant agreement no. 633053. The views and opinions expressed herein do not necessarily reflect those of the European Commission.

References

[1] J. Linke, Fusion Sci. Technol. 49 (2006) 455–464.
[2] A. Raffray, R. Nygren, D. Whyte, S. Abdel-Khalik, R. Doerner, F. Escourbiac, T. Evans, R. Goldston, D. Hoelzer, S. Konishi, P. Lorenzetto, M. Merola, R. Neu, P. Norajitra, R. Pitts, M. Rieth, M. Roedig, T. Rognlien, S. Suzuki, M. Tillack, C. Wong, Fusion Eng. Des. 85 (2010) 93–108.
[3] G. Pintsuk, A. Prokhodtseva, I. Uytdenhouwen, J. Nucl. Mater. 481–486 (2011) 417.
[4] M. Wirtz, J. Linke, G. Pintsuk, L. Singheiser, I. Uytdenhouwen, Phys. Scr. T145 (2011) 014058.
[5] J. Linke, T. Loewenhoff, V. Massaut, G. Pintsuk, G. Ritz, M. Roedig, A. Schmidt, C. Thomser, I. Uytdenhouwen, V. Vasechko, M. Wirtz, Nucl. Fusion 51 (2011) 073017.
[6] S. Pestchanyi, J. Linke, Fusion Eng. Des. 82 (2007) 1657–1663.
[7] A. Arakcheev, A. Huber, M. Wirtz, G. Sergienko, I. Steudel, A. Burdakov, J. Coenen, A. Kreter, J. Linke, P. Mertens, A. Shoshin, B. Unterberg, A. Vasilyev, J. Nucl. Mater. 463 (2015) 246–249.
[8] M. Li, M. Sommerer, E. Werner, S. Lampenscherf, T. Steinkopff, P. Wolfrum, J.-H. You, Eng. Fract. Mech. 135 (2015) 64–80.
[9] M. Li, E. Werner, J.-H. You, J. Nucl. Mater. 457 (2015) 256–265.
[10] M. Li, E. Werner, J.-H. You, Nucl. Mater.Energy 2 (2015) 1–11.
[11] Dassault Systèmes, ABAQUS 6.14 Documentation, Dassault Systèmes, Providence, RI, USA, 2014.
[12] ITER, ITER Material Properties Handbook, ITER Document No.G74 M 16, ITER, 2005.
[13] ITER, ITER Structural Design Criteria for In-Vessel Components (SDC-IC). Appendix A: Materials Design Limit Data, ITER, 2012.
[14] Y. Lei, Proceedings of the 23rd Conference on Structural Mechanics in Reactor Technology, Manchester, United Kingdom, 2015.
[15] E. Gaganidze, D. Rupp, J. Aktaa, J. Nucl. Mater. 446 (2014) 240–245.

Please cite this article as: M. Li, J.-H. You, Cracking behavior of tungsten armor under ELM-like thermal shockloads II: A revised prediction for crack appearance map, Nuclear Materials and Energy (2016), http://dx.doi.org/10.1016/j.nme.2016.02.001